ACS OMEGA

http://pubs.acs.org/journal/acsodf

Article

Palladium-Supported Polydopamine-Coated $NiFe_2O_4$@TiO_2: A Sole Photocatalyst for Suzuki and Sonogashira Coupling Reactions under Sunlight Irradiation

Prashanth Goud Banda and Raghasudha Mucherla*

Cite This: *ACS Omega* 2022, 7, 29356−29368

Read Online

ACCESS | Metrics & More | Article Recommendations | Supporting Information

ABSTRACT: The effective utilization of solar energy in synthetic organic chemistry has gained extensive attention owing to its enormous energy and environmentally benign nature. In this context, we designed and synthesized a magnetically retrievable, sole palladium (Pd)-supported polydopamine-coated core@shell ($NiFe_2O_4$@TiO_2) heterogeneous nanophotocatalyst for Suzuki and Sonogashira coupling reactions under sunlight irradiation. The synthesized catalyst was characterized by powder X-ray diffraction (PXRD), Fourier-transform infrared, UV−vis, scanning electron microscopy, energy-dispersive X-ray spectroscopy, transmission electron microscopy, X-ray photoelectron spectroscopy, and vibrating sample magnetometer analysis. The photocatalytic activity of the synthesized nanocatalyst under sunlight irradiation was assessed for both Suzuki and Sonogashira coupling reactions, where it worked excellently well with a high yield of the product up to 98 and 96%, respectively. Its efficacy was also investigated in the conversion of substituted substrates in both the coupling reactions into desired biaryls and diarylacetylenes. Unique features of the synthesized catalyst are (i) its effective performance for both the aforesaid coupling reactions under ambient reaction conditions for a short reaction time in polar protic solvents (ethanolic water/EtOH) with good yield without any byproduct, (ii) magnetic retrieval of the catalyst from the reaction mixture employing an external magnet is an added advantage, and (iii) the retrieved catalyst could potentially be reutilized for up to five consecutive runs without appreciable diminution of catalytic efficacy, and its stability was confirmed by inductively coupled plasma optical emission spectroscopy analysis and XRD.

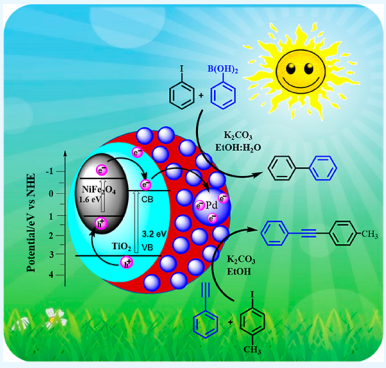

1. INTRODUCTION

Solar energy has considerable potential as a green energy resource owing to its superabundance, cost efficiency, and non-polluting nature. The use of sunlight to carry out chemical reactions, frequently named photo-catalysis, is a significant method to harness solar energy.[1−3] It shows good potency in a number of chemical processes such as photocatalytic degradation of pollutants, photocatalyzed organic reactions in the presence of various nanostructures, and so forth.[4−6] Two important phenomena in the photocatalysis process are efficient photogeneration of the electron−hole (e^-−h^+) pair and their separation.[7,8] The use of photo-generated holes or electrons for oxidation or reduction of organic molecules is an important aspect in light-driven chemical reactions. Regardless, the simultaneous application of both the photo-generated e^-−h^+ pairs for organic chemical reactions provides an outstanding catalytic perspective for cost-efficient and environmentally benign synthesis. Very limited reports are available on this aspect, and it has grabbed the attention of researchers to take it as a challenge in synthetic organic chemistry.[9−11]

Organic reactions involving C−C bond coupling (Suzuki and Sonogashira) are extremely significant with convenient approaches in synthetic organic chemistry in the preparation of natural products, pharmaceutical drugs, functional conjugated organic molecular materials, and so forth.[12−15] The traditional way of carrying out coupling reactions is the homogeneous catalysis using Pd/Pd complexes.[16] The notable limitations associated with the homogeneous Pd/Pd complex catalyst are its non-reusability, air and water sensitivity, and product contamination by residual Pd/ligands, thus making it inseparable.[17] These limitations accompanying the homogeneous catalysis motivated the scientific community to develop novel approaches in the form of heterogeneous catalysis with a focus on catalyst recovery and reuse.[18−21] Thus, development of eco-friendly heterogeneous photocatalysts for various organic coupling reactions with excellent stability, reusability, separability, and activity under ambient reaction conditions is crucial for synthetic organic applications.[22,23]

For the efficacious harvest of solar energy, several photocatalysts have been developed. TiO_2 is a well-known photocatalyst, but its usage is restricted due to a wide band

Received: June 9, 2022
Accepted: July 19, 2022
Published: August 11, 2022

https://doi.org/10.1021/acsomega.2c03603
ACS Omega 2022, 7, 29356−29368

gap (3.2 eV) that falls in the UV region. Due to environmental concerns, there is an urgency to perform the photocatalytic activity under visible light irradiation.[24−26] Consequently, the photocatalyst that absorbs visible light and that can be easily separable from the reaction mixture is the pressing priority. Incorporating magnetic materials into solid matrices is the best choice that enables the integration of prominent methods for both photo-catalysis and magnetic separation.[27] Among the magnetic materials, spinel ferrites have extraordinary properties such as a low band gap, good stability against photo-corrosion, unique superparamagnetic nature, easy preparation, low cost, high adsorption capacity, and so forth.[28] Among the magnetic spinel ferrites, $NiFe_2O_4$, as an n-type semiconductor with a low band gap (∼1.63 eV), has attracted much attention due to its effective light absorption capacity and stable physical and chemical properties. In accordance with the aforesaid facts, it is expected and reported that the integration of TiO_2 (high band gap) with $NiFe_2O_4$ (low band gap) leads to a core−shell material with a tuned band gap for visible light absorption. The resulting material thus possesses better magnetic separation for use as a good photocatalyst.[29,30]

To make this photocatalyst suitable for Suzuki and Sonogashira coupling reactions, we propose incorporating Pd nanoparticles (NPs) onto the $NiFe_2O_4$@TiO_2 core@shell material owing to the effectiveness of Pd in catalyzing the coupling reactions. For the past few years, it has been reported that the supported Pd NPs have been explored to be a substitute for Pd complexes as a catalyst to overcome its limitations.[31−34] For good binding of Pd particles on the surface of the catalyst, it is an established fact that polydopamine (PDA) could be used as a universal surface modifying agent. It is because of the fact that PDA can form coordinate bonds with transition metal ions via its N- and O-binding sites, which can easily be reduced to metal NPs. Thus, it results in the formation of metal-supported PDA that could be used as an effective catalyst.[35−37]

Reports on the availability of a sunlight-driven sole magnetic photocatalyst under ambient conditions for both Suzuki and Sonogashira coupling reactions are scarce. Hence, in the present work, we propose to synthesize Pd(0) NPs supported on PDA-coated $NiFe_2O_4$@TiO_2 ($NiFe_2O_4$@TiO_2@PDA-Pd) as a nanophotocatalyst for C−C coupling reactions. Pd(0) NPs can be supported on the $NiFe_2O_4$@TiO_2@PDA material via a simple method involving immersion of Pd(II) ions in $NiFe_2O_4$@TiO_2@PDA followed by their reduction with sodium borohydride. In Suzuki and Sonogashira coupling reactions, this catalyst is expected to exhibit effective photocatalytic activity under sunlight absorption and is validated in the present work. Furthermore, the $NiFe_2O_4$@TiO_2@PDA-Pd can be easily separated with an external magnet for its reusability, without appreciable loss in catalytic efficacy.

2. EXPERIMENTAL SECTION

2.1. Materials. Ferric nitrate (Finar, 99%); nickel nitrate (Finar, 99%); titanium(IV) isopropoxide (Sigma-Aldrich, 99%); dopamine hydrochloride (98%); $PdCl_2$ (Sigma-Aldrich, 99%); $NaBH_4$ (Finar, 99%); NaOH (Finar, 96%); HNO_3 (Finar, 69%); methanol (MeOH, Finar, 99%); ethanol (EtOH, Finar, 99%); ethyl acetate (EtAC, Finar, 99%); and *n*-hexane (Finar, 98%) were used as starting materials, and double distilled (DD) water was used all through the experiments.

2.2. Synthesis of $NiFe_2O_4$ NPs. Nickel ferrite ($NiFe_2O_4$) NPs were synthesized using the hydrothermal method. In this method, $Ni(NO_3)_2{\cdot}6H_2O$ and $Fe(NO_3)_3{\cdot}9H_2O$ were taken in a 1:2 ratio and dissolved in 40 mL of DD water. A clear solution was obtained after 15 min of stirring at room temperature (RT). The pH of the solution was adjusted to 12 using 2 M NaOH solution with continuous stirring for 30 min. The resulting solution was placed in a stainless-steel autoclave and was heated at 180 °C for 12 h. Then, it was allowed to cool to RT. The attained product was washed three times with DD water and ethanol, followed by drying in an oven at 60 °C. Finally, it was subjected to calcination at 800 °C for 2 h. Thus, $NiFe_2O_4$ NPs were prepared.

2.3. Synthesis of $NiFe_2O_4$@TiO_2 (core@shell) NPs. Initially, 1 g of synthesized nickel ferrite ($NiFe_2O_4$) was dispersed in 50 ml of methanol. The mixture was magnetically stirred for 15 min. 2.5 g of titanium tetraisopropoxide [yield of TiO_2 (anatase): 1 g] was then introduced into the mixture and stirred for 10 min, followed by the addition of 10 mL of DD water. After 10 min, HNO_3 was added slowly to maintain the pH of the solution at 2. The resulting solution was continuously stirred for 90 min, turning into a gel-like material. The gel was dried in an oven at 60 °C for 1 h and calcined at 500 °C for 2 h. $NiFe_2O_4$@TiO_2 NPs were thus prepared.

2.4. Surface Modification of $NiFe_2O_4$@TiO_2 with PDA. 1 g of synthesized $NiFe_2O_4$@TiO_2 NPs was added to 500 mL of Tris buffer (10 mM, pH 8.5). 1 g of dopamine was then introduced into the resulting solution. The resulting mix was mechanically stirred at RT for 24 h. During the process, dopamine was polymerized to PDA and got coated over $NiFe_2O_4$@TiO_2, resulting in the formation of $NiFe_2O_4$@TiO_2@PDA NPs. PDA-coated $NiFe_2O_4$@TiO_2 was separated employing an external magnet at the end of the reaction and was washed with DD water and ethanol, followed by drying in an oven at 40 °C to form the surface-modified $NiFe_2O_4$@TiO_2 with PDA.

2.5. Synthesis of the $NiFe_2O_4$@TiO_2@PDA-Pd Catalyst. 1 g of synthesized $NiFe_2O_4$@TiO_2@PDA was dispersed in 200 mL of DD water for 20 min. Subsequently, 0.05 g of $PdCl_2$ in 20 mL of water was introduced into the reaction mixture with stirring for 24 h. Consequently, with vigorous stirring, 0.05 g of $NaBH_4$ was added to the reaction mixture. During the process, Pd(II) got reduced to Pd(0) and deposited on $NiFe_2O_4$@TiO_2@PDA. After 1 h of stirring, the resulting Pd-supported $NiFe_2O_4$@TiO_2@PDA ($NiFe_2O_4$@TiO_2@PDA-Pd) was isolated with the aid of an external magnet, washed thoroughly with DD water, and then dried at 60 °C under vacuum for 12 h.

2.6. Photocatalytic Suzuki Coupling Reaction. The photocatalytic activity of the prepared catalyst for a typical Suzuki coupling reaction (SCR) between aryl halides and arylboronic acid was investigated. In this process, aryl halides (1 mmol), arylboronic acid (1.5 mmol), K_2CO_3 (2.5 mmol), and the $NiFe_2O_4$@TiO_2@PDA-Pd catalyst (5 mg) were mixed in a round-bottom (RB) flask with 3 mL of EtOH and H_2O as a solvent in a 1:1 volume ratio. The reaction mixture was continuously stirred under direct sunlight from 11.00 am to 3.00 pm. The average intensity of the sunlight was measured to be 50−60 mW/cm^2 using a Newport Optical Power Meter (model 842.PE) with an average outdoor temperature of 30 °C. On completion of the reaction [as confirmed by thin-layer chromatography (TLC)], the catalyst was isolated by simple means with the aid of a magnet. After being extracted twice with ethyl acetate, the products were purified using column chromatography. ^{1}H and ^{13}C NMR spectral analysis was

https://doi.org/10.1021/acsomega.2c03603
ACS Omega 2022, 7, 29356−29368

Scheme 1. Preparation Path of the $NiFe_2O_4$@TiO_2@PDA-Pd Nanophotocatalyst

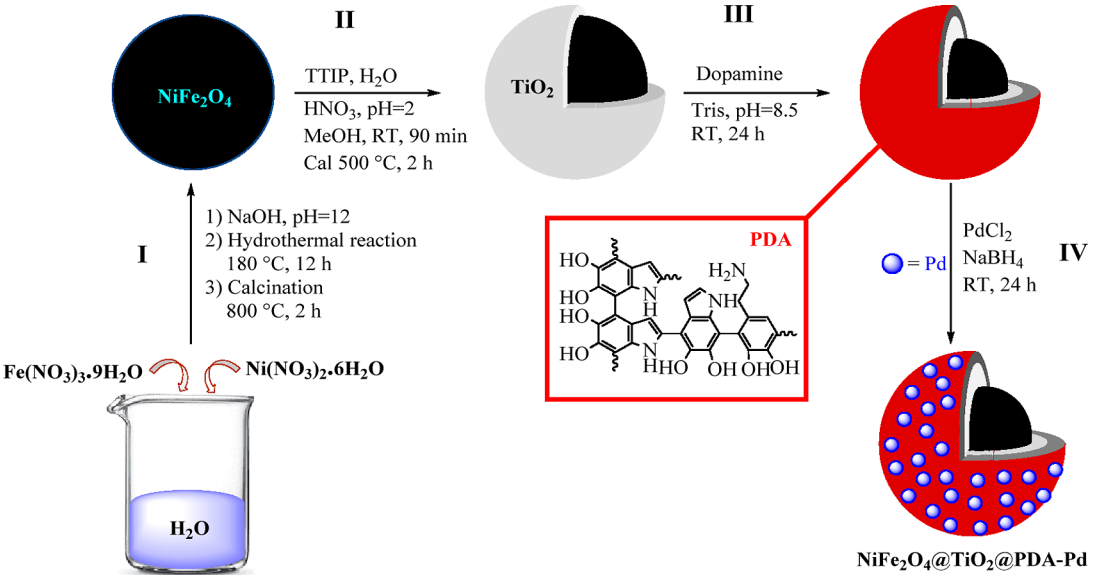

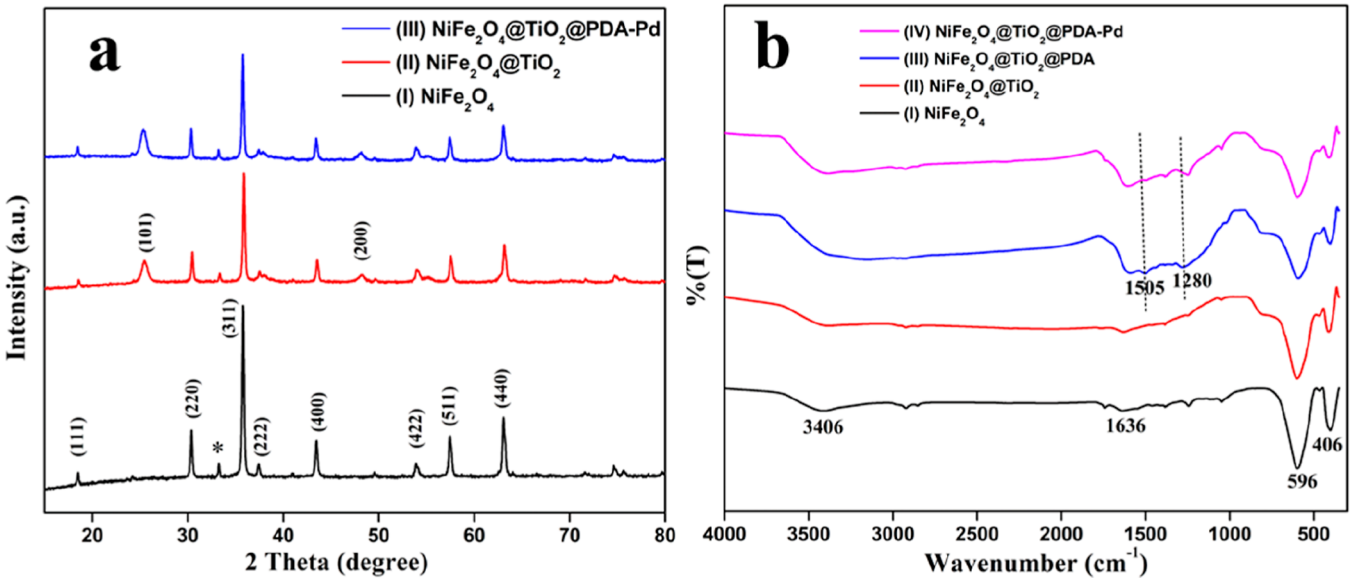

Figure 1. (a) XRD spectra and (b) FTIR spectra of samples.

performed to analyze the products. The separated catalyst was thoroughly washed with DD water and ethanol (three times) for recycling applications, and the dried catalyst (at 60 °C overnight) was used in the next run.

2.7. Photocatalytic Sonogashira Coupling Reaction. The photocatalytic performance of the prepared catalyst for a typical Sonogashira coupling reaction between aryl halides and arylacetylene to yield diarylacetylene was investigated. In this experiment, aryl halides (1 mmol), arylacetylene (1.3 mmol), K_2CO_3 (2 mmol), and the $NiFe_2O_4$@TiO_2@PDA-Pd catalyst (10 mg) were mixed in an RB flask with 3 mL of the EtOH solvent. The reaction was continuously stirred under the irradiation of sunlight at an average outdoor temperature of 30 °C. On completion of the reaction (as confirmed by TLC), the catalyst was set apart with the aid of a magnet. After being extracted twice with ethyl acetate, the products were purified using column chromatography. ^1H and ^{13}C NMR spectral analysis was performed to analyze the products. The separated catalyst was washed with DD water and ethanol for recycling applications, and the dried catalyst (at 60 °C overnight) was used in the next run.

2.8. Characterization of the Catalyst. Powder X-ray diffraction (PXRD) analysis of the synthesized materials ($NiFe_2O_4$, $NiFe_2O_4$@TiO_2, and $NiFe_2O_4$@TiO_2@PDA-Pd) was carried out on a PAN Analytical Advance X-ray diffractometer with Ni-filtered Cu Kα (λ = 1.5406 Å) radiation in a 2θ scan range between 10 and 60° to assess the crystalline nature of the catalyst. The Fourier-transform infrared (FT-IR) spectrum for all the materials was recorded in the range of 4000−400 cm^{-1} using the PerkinElmer Spectrum using the KBr pellet technique. The surface morphology of the synthesized photocatalyst was examined using scanning electron microscopy (SEM, Carl Zeiss SMT Ltd., Zeiss EVO 18), transmission electron microscopy (TEM), and selected area electron diffraction (SAED) (TEM, Jeol/JEM 2100 at 200 kV). X-ray photoelectron spectroscopy (Kratos/Shimadzu

https://doi.org/10.1021/acsomega.2c03603
ACS Omega 2022, 7, 29356−29368

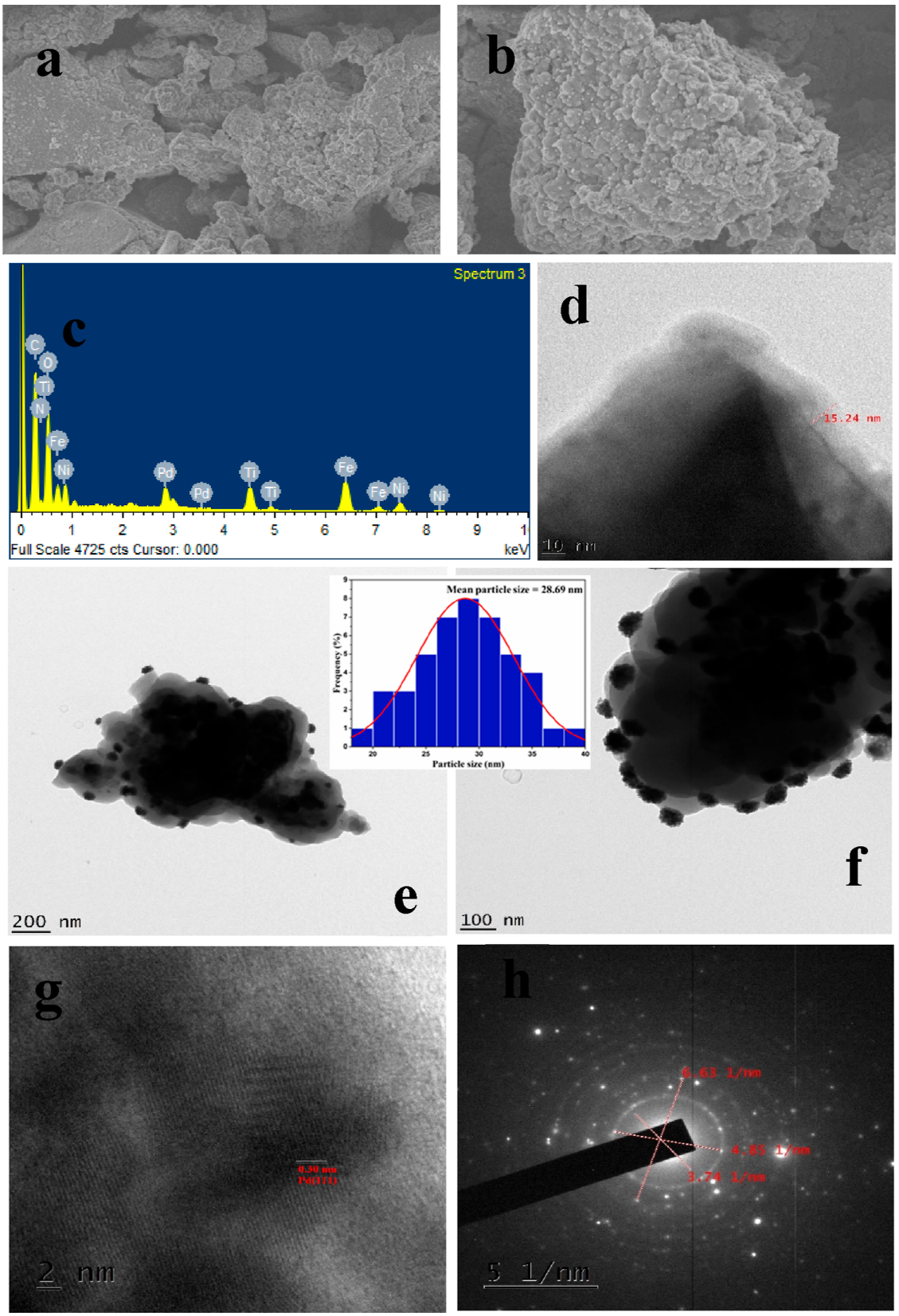

Figure 2. (a,b) SEM images, (c) EDX, (d) PDA layer, (e,f) TEM images with a particle size histogram, (g) HRTEM image, and (h) SAED pattern of $NiFe_2O_4$@TiO_2@PDA-Pd.

Amicus, Model: ESCA 3400) was used to determine the binding energies of elements in the catalyst. UV−vis diffuse reflectance spectra of all the materials was recorded on Analytik Jena, SPECORD 210 PLUS at RT. The magnetic hysteresis curves of the catalyst were recorded using a vibrating sample magnetometer (VSM, Lake Shore, Model: 8600

https://doi.org/10.1021/acsomega.2c03603
ACS Omega 2022, 7, 29356−29368

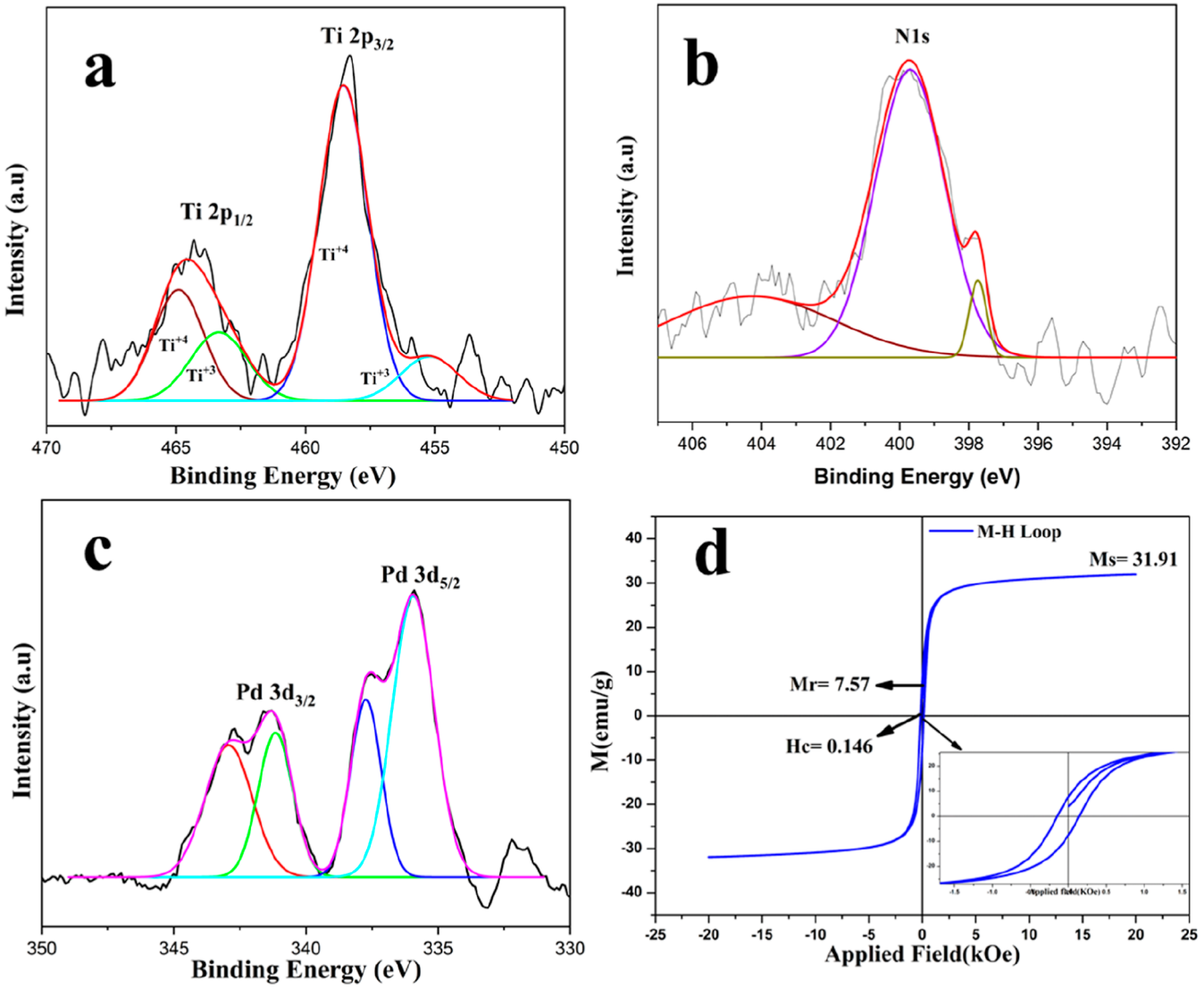

Figure 3. (a) Ti 2p peaks, (b) N 1s peak, (c) Pd 3d peaks, and (d) magnetization curve of $NiFe_2O_4$@TiO_2@PDA-Pd; inset: zoomed-in region of the area under the curve.

Series). Inductively coupled plasma optical emission spectroscopy (ICP-OES) analysis was aimed to ascertain the quantity of Pd in the synthesized nanocatalyst (PerkinElmer Optima 5300 DV). ^{1}H NMR and ^{13}C NMR spectra were recorded on an ADVANCED-III Bruker 400 MHz NMR spectrometer using $CDCl_3$ as the solvent and tetramethylsilane as an internal standard where chemical shifts are mentioned as parts per million (ppm).

3. RESULTS AND DISCUSSION

3.1. Preparation of the $NiFe_2O_4$@TiO_2@PDA-Pd Catalyst. The $NiFe_2O_4$@TiO_2@PDA-Pd catalyst was synthesized by a multistep procedure (Scheme 1). In step I, the $NiFe_2O_4$ NPs were prepared by the hydrothermal method. In step II, the in situ $NiFe_2O_4$@TiO_2 core@shell structure was prepared via the sol−gel method. In step III, $NiFe_2O_4$@TiO_2 NPs were surface-modified by PDA where dopamine was polymerized in Tris buffer solution (10 mM, pH 8.5) under continuous stirring. Finally, in step IV, palladium(0) NPs were supported on $NiFe_2O_4$@TiO_2@PDA by impregnation of Pd(II) ions over the surface of the polymer (PDA) layer followed by its subsequent reduction with sodium borohydride. This led to the synthesis of the palladium-supported PDA-coated core@shell nanophotocatalyst ($NiFe_2O_4$@TiO_2@PDA-Pd). An external magnet was used to isolate the synthesized photocatalyst, which was then dried under vacuum conditions for further use. The overall synthesis of the nanophotocatalyst is depicted in Scheme 1.

3.2. Characterization of the $NiFe_2O_4$@TiO_2@PDA-Pd Catalyst. The indexed XRD patterns of the synthesized $NiFe_2O_4$, $NiFe_2O_4$@TiO_2, and the $NiFe_2O_4$@TiO_2@PDA-Pd catalyst are shown in Figure 1. The broad peaks observed in the figure reveal the nanoscale range of the particles possessing a small crystallite size. The observed peaks in Figure 1a(I) at 2θ values of 18.5, 30.4, 35.8, 37.3, 43.4, 53.8, 57.4, and 63.0° are attributed to (111), (220), (311), (222), (422), (511), and (440) diffractions, respectively, signifying the formation of single-phase pure crystalline spinel $NiFe_2O_4$ (ICDD card no. 10−0325). A small peak was detected in the figure at 2θ of 33.2° for the $NiFe_2O_4$ sample calcined at 800 °C, which corresponds to a small quantity of the impure phase of α-Fe_2O_3 that occurs naturally as hematite (ICDD card 33-0664).[38] The additional peaks appeared at 2θ of 25.3 and 48.1°

https://doi.org/10.1021/acsomega.2c03603
ACS Omega 2022, 7, 29356−29368

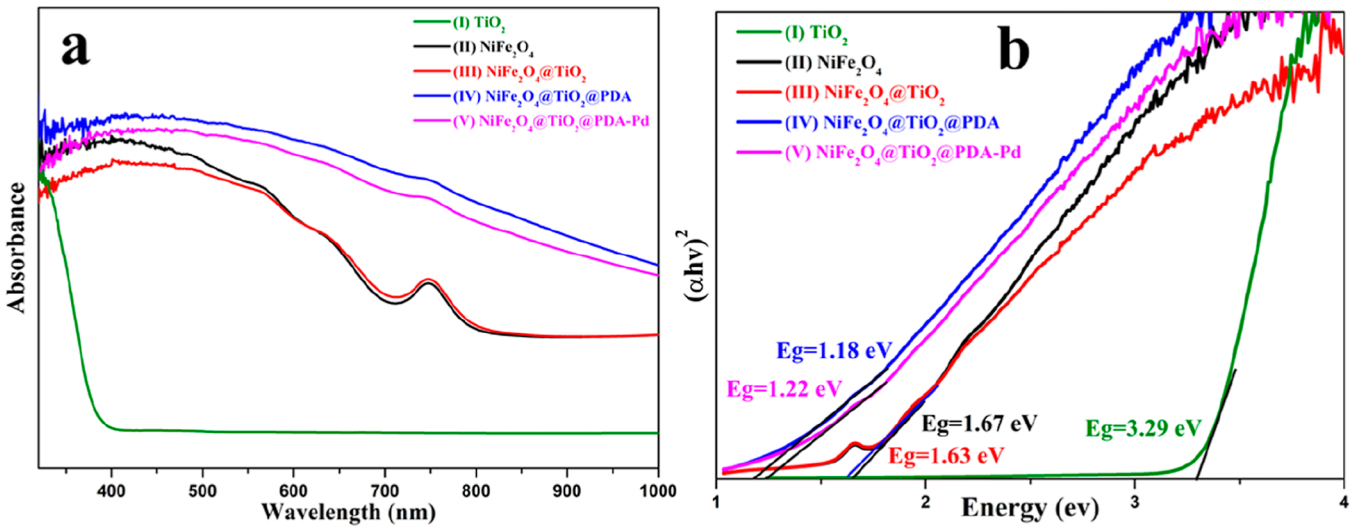

Figure 4. (a) UV−vis absorption spectra and (b) band gap energies of the samples.

along with the diffraction peaks of $NiFe_2O_4$ in Figure 1a(II) attributed to (101), (200) diffractions of anatase (JCPDS card no. 78-2486), thus signifying the formation of $NiFe_2O_4$@TiO_2 NPs.[39] The diffraction patterns of the catalyst in Figure 1a(III) depict that the crystallinity of $NiFe_2O_4$@TiO_2 NPs was intact and not altered despite the PDA coating and Pd loading as well. Also, Figure 1a(III) has no noticeable peak related to Pd NPs owing to the low palladium content on the PDA surface.

FT-IR spectra of the prepared samples are shown in Figure 1b. Two significant peaks were noticed in the range of 600−400 cm^{-1} for all the samples characteristic of the spinel structure. The peaks detected at 406 and 596 cm^{-1} correspond to the intrinsic vibrations of metal ion−oxygen complexes in octahedral and tetrahedral sites in the spinel structure, respectively, and the peaks around ∼1600 and ∼3400 cm^{-1} represent the bending and stretching mode of surface-adsorbed H_2O and also the stretching mode of OH groups [Figure 1b(I)]. The peaks that appeared at 1505 and 1280 cm^{-1} in Figure 1b(III), which are not seen in Figure 1b(I,III), were attributed to C═C stretching and C−N stretching modes, respectively, that indicated the presence of −C═C−NH functional groups of PDA. The observed peak at around ∼3390 cm^{-1} indicates the presence of −OH of phenol in $NiFe_2O_4$@TiO_2@PDA. These outcomes infer that PDA has been successfully deposited on the surface of $NiFe_2O_4$@TiO_2 NPs by its adsorption. In the FTIR spectrum of the $NiFe_2O_4$@TiO_2@PDA-Pd nanocatalyst, no dramatic changes were observed as evident from Figure 1b(IV). Meanwhile, the peak intensity observed at 1505 and 1280 cm^{-1} has shifted to a low frequency owing to the bonding interactions between the PDA functional groups and the Pd NPs.[40,41]

The surface morphology of the synthesized nanocatalyst $NiFe_2O_4$@TiO_2@PDA-Pd was observed by SEM images shown in Figure 2a,b that represents a near spherical cluster-like structure of the catalyst. Keen examination of the image depicts the presence of small particles supported on a continuous layer over a core−shell justifying the immobilization of Pd NPs on the PDA layer over the $NiFe_2O_4$@TiO_2 core−shell structure as $NiFe_2O_4$@TiO_2@PDA-Pd. Furthermore, the energy-dispersive X-ray spectroscopy (EDX) detector attached to SEM was used to establish the existence of Pd particles over PDA on $NiFe_2O_4$@TiO_2 NPs. The SEM−EDX spectrum shown in Figure 2c describes the presence of Pd, N, Ti, Fe, Ni, C, and O elements in the catalyst. Thus, the SEM−EDX images portray the successful coating of PDA on $NiFe_2O_4$@TiO_2 and also effective loading of Pd over the surface of $NiFe_2O_4$@TiO_2@PDA. Accumulation of Pd NPs on the surface of PDA in the catalyst was also confirmed by TEM analysis. TEM images portray a spherical shape of the NPs in the catalyst, thus further confirming the morphology observed by SEM. The TEM image in Figure 2d reveals the presence of a thin continuous PDA layer around $NiFe_2O_4$@TiO_2 with a thickness of about 15.24 nm. The two TEM images shown in Figure 2e,f noticeably represent the thick and uniform distribution of small Pd NPs throughout the PDA surface. They depict the magnified images at 100 and 200 nm where Pd NPs are homogeneously decorated on the peripheral surface of NiFe2O4@TiO2@PDA without large agglomeration, inferring that Pd NPs are effectively immobilized on the surface of PDA.

The particle size distribution histogram of the catalyst which is embedded in Figure 2e,f estimated the average size of the Pd NPs to be around 28.6 nm. It was found that the dark Pd NPs were coated over the gray PDA layer on the dark core−shell of $NiFe_2O_4$@TiO_2. These TEM images are in accordance with SEM information with respect to the morphology. The high-resolution TEM (HRTEM) image shown in Figure 2g is indicative of the number of grains with different orientation of the planes, thus confirming the polycrystalline nature of the material. The lattice fringe spaces of 0.30 nm shown in the figure could possibly be ascribed to the (111) crystal plane of Pd NPs. The SAED pattern of $NiFe_2O_4$@TiO_2@PDA-Pd is depicted in Figure 3h. It shows diffraction rings composed of a bright spot possessing sixfold symmetry that manifests the polycrystalline nature of the material.

X-ray photoelectron spectroscopy (XPS) was employed to confirm the effective coordination of Pd on the PDA layer. It is a powerful tool to understand the electronic properties of the coordinated particles on the surface such as the electron environment, binding energy, and chemical valence states of the metals. The XPS spectra of the $NiFe_2O_4$@TiO_2@PDA-Pd nanophotocatalyst are shown in Figure 3 where the chemical valence states of Ti, N, and Pd in the catalyst were analyzed.

The two noticeable bands at binding energies 458.4 and 464.9 eV were ascribed to the Ti $2p_{3/2}$ and Ti $2p_{1/2}$

https://doi.org/10.1021/acsomega.2c03603
ACS Omega 2022, 7, 29356−29368

photoelectrons in the Ti^{4+} chemical state, respectively, whereas the two peaks at 455.4 and 463.4 eV were attributed to the Ti $2p_{3/2}$ and Ti $2p_{1/2}$ photoelectrons in the Ti^{3+} state in the TiO_2 chemical state, respectively (Figure 3a).[42] The peak at 399.7 eV in Figure 3b represents the N1s photoelectrons of the NH group. It is evident from the N1s spectrum of Figure 3b that the $NiFe_2O_4$@TiO_2 core@shell NPs were successfully coated with PDA. Furthermore, the two observed bands at binding energies 335.3 and 340.6 eV in Figure 3c can be indexed as Pd(0) $3d_{5/2}$ and Pd(0) $3d_{3/2}$, respectively. These values confirm the presence of Pd(0) in the prepared catalyst which was not noticeable in XRD. These results were in accordance with the values of metallic Pd.[43] The magnetic performance of the synthesized nanocatalyst was investigated with the VSM at RT. Figure 3d demonstrates the magnetization curve of the $NiFe_2O_4$@TiO_2@PDA-Pd catalyst. From the figure, the saturation magnetization (M_s), coercivity (H_c), and remanence magnetization (M_r) are found to be 31.9 emu/g, 0.146 kOe, and 7.57 emu/g, respectively. The magnetization data reveals the good magnetic behavior of the synthesized catalyst, thus becoming evidential of the magnetic recovery and reusability of the catalyst.

The UV−vis diffuse reflectance spectra of the synthesized $NiFe_2O_4$, $NiFe_2O_4$@TiO_2, $NiFe_2O_4$@TiO_2@PDA, $NiFe_2O_4$@TiO_2@PDA-Pd, and pure TiO_2 were recorded, and the results are depicted in Figure 4a. It is obvious from the figure that pure TiO_2 and $NiFe_2O_4$ show absorption bands with absorption edges at 400 and 700 nm, respectively, as illustrated in Figure 4a(I,II), indicating the absorption of TiO_2 in the UV region and that of $NiFe_2O_4$ in the visible region. However, after the surface modification of $NiFe_2O_4$ with TiO_2, the obtained core@shell ($NiFe_2O_4$@TiO_2) material also exhibited the band with the absorption edge in the visible region as seen in Figure 4a(III), confirming the ability of $NiFe_2O_4$@TiO_2 to absorb visible light. Even after coating $NiFe_2O_4$@TiO_2 with PDA and also supported by the metal (Pd) on its surface, the resulting $NiFe_2O_4$@TiO_2@PDA-Pd magnetic photocatalyst still exhibits absorption in the visible region as evident from Figure 4a(IV,V). The band gap energy (E_g) of all the samples was estimated from the Tauc plot of $(\alpha h\upsilon)^2$ versus $h\upsilon$ as presented in Figure 4b. Extrapolation of the $h\upsilon$ value to $\alpha = 0$ results in absorption band gap energy (E_g). As seen from Figure 4b, E_g for pure $NiFe_2O_4$ and TiO_2 was found to be 1.67 and 3.29 eV, respectively, which is in accord with the reported values.[44,45] In contrast, the band gap energy of $NiFe_2O_4$@TiO_2 was observed to be 1.63 eV which indicates the absorption in the visible region. Furthermore, the decrease in energy gap (E_g) upon core@shell formation confirms the electronic coupling between $NiFe_2O_4$ and TiO_2. After surface modification with PDA supported by the Pd metal, an even stronger visible-region band gap energy of 1.22 eV was observed for the $NiFe_2O_4$@TiO_2@PDA-Pd nanocatalyst.

3.3. Application of the $NiFe_2O_4$@TiO_2@PDA-Pd Catalyst in Suzuki and Sonogashira Coupling Reactions under Sunlight. In the past few decades, Pd has been employed as an active catalyst for C−C coupling reactions. Nevertheless, most of the times, the coupling reactions with Pd as a catalyst take place under heating conditions, which consumes lot of energy. Therefore, it would be a significant improvement if we could improve the catalytic activity of Pd as a catalyst at ambient temperatures using the visible region of the sunlight which is an abundant and environmentally sustainable energy source. As our synthesized catalyst shows absorption in the visible region, we tried to test the validity of our catalyst for the Suzuki and Sonogashira coupling reactions under natural sunlight under ambient conditions (photocatalytic coupling reactions).

3.3.1. Suzuki Coupling Reaction. A simple SCR involving aryl halides and arylboronic acid was performed using the synthesized $NiFe_2O_4$@TiO_2@PDA-Pd nanophotocatalyst under sunlight, at an average outdoor temperature of 30 °C. Optimization of various vital reaction conditions for the SCR, viz., nature of the solvent, base, light source, and Wt % of Pd, was performed. The effect of various solvents in the presence of K_2CO_3 as a base with 5% of Pd by weight on the photocatalytic SCR was observed. The obtained yield of the product was low in the presence of polar aprotic solvents, namely, dimethyl sulfoxide and dimethylformamide, and also in the presence of nonpolar solvents such as toluene (Table S1, entries 1−3). However, observed yield of the product was high in the presence of polar protic solvents such as ethanol and methanol (Table S1, entries 4,5). Furthermore, the reaction in pure H_2O resulted in moderate yield (Table S1, entry 6) of the product. It was observed that 98% yield of the product was obtained in the presence of a mixture of EtOH and H_2O as a solvent in a 1:1 ratio, indicating the significant enhancement in the photocatalytic activity (Table S1, entry 7). These results infer that photocatalyzed Suzuki reactions in the presence of the $NiFe_2O_4$@TiO_2@PDA-Pd nanophotocatalyst require protic solvents. Furthermore, the influence of other bases (Cs_2CO_3, NaOH, Et_3N) (Table S1, entries 12−14) in the solvent EtOH·H_2O (1:1) was also explored, but good yield was observed in the presence of only K_2CO_3 as a base among all (Table S1, entry 7).

To study the influence of light on the SCR, the reaction was performed in dark at RT and also at 60 °C. It was found that moderate yields (30 and 64%) (Table S1, entries 15,16) were obtained in dark at RT and at 60 °C, respectively. While performing the reaction under visible light (Hg lamp 250W), the product yield was improved (85%) (Table S1, entry 17). To test the feasibility of environmental concerns, the reaction was initiated in natural sunlight, and an excellent yield (98%) of the product was observed. Furthermore, no product was observed in the presence of $NiFe_2O_4$, $NiFe_2O_4$@TiO_2, and $NiFe_2O_4$@TiO_2@PDA separately. Thus, this study indicates the significance of Pd presence in the synthesized nanocatalyst ($NiFe_2O_4$@TiO_2@PDA-Pd) in carrying out the SCR.

The choice of Pd loading as 5% by weight in all the aforementioned optimization experiments was made based on the previously reported values in different catalysts.[40,41] Even though we got good yield (98%) with 5% loading of Pd, to test the effect of Pd loading, we performed the reaction, and the yield was monitored with different Pd loadings such as 1, 2.5% (<5%), and with 7.5% (>5%) for the same reaction time as that of 5% Pd loading (Table 1). Low yield was observed with 1 and 2.5% (30% and 65%, respectively), whereas the same yield (98%) was observed with 7.5%. Thus, the efficacy of the catalyst in the coupling reaction was proved to be good with a Pd loading of 5% by weight (Table 1, entry 3).

The reaction generality was further investigated by $NiFe_2O_4$@TiO_2@PDA-Pd under the sunlight using several aryl halides and substituted arylboronic acids to validate the scope of the synthesized catalyst (Table 2). It is observed that the presence of electron-withdrawing groups (EWGs) and electron-donating groups (EDGs) produces outstanding yields for para-substituted aryl halides. The reaction progressed

https://doi.org/10.1021/acsomega.2c03603
ACS Omega 2022, 7, 29356−29368

Table 1. Influence of Catalyst Loading on the Suzuki Coupling Reaction[a]

S. No.	catalyst loading (wt %)	yield (%)[b]
1	1	30
2	2.5	65
3	**5**	**98**
4	7.5	98

[a]Reaction conditions: iodo benzene (1.0 mmol), phenyl boronic acid (1.5 mmol), $NiFe_2O_4$@TiO_2@PDA-Pd catalyst (5 mg), and K_2CO_3 (2.5 mmol) in EtOH·H_2O (3 mL) under sunlight at 30 °C for 0.5 h. [b]Isolated yields.

effectively regardless of substrates with the EWG and EDG yielding more than 85% in most of the cases, except in case of aryl bromides and chlorides due to the stronger C−halogen bond than the C−I bond (Table 2, entries 10−12). Furthermore, it was observed that the reaction progressed faster on substrates with EDGs than on substrates with EWGs. This fact could be addressed by the inductive effects of the substituent groups on the substrates.[46]

3.3.2. Sonogashira Coupling Reaction. The catalytic potential of the synthesized $NiFe_2O_4$@TiO_2@PDA-Pd catalyst with 5% by weight of Pd loading was further extended to test the feasibility of the Sonogashira coupling reaction involving aryl halides and arylacetylenes under sunlight, at an average outdoor temperature of 30 °C. Optimization of various vital reaction conditions, viz., nature of the solvent, base, and light source for the Sonogashira reaction, was performed. In this reaction, the solvent played a significant role. EtOH was found to be an excellent solvent for this reaction out of a variety of solvents tested (Table S2, entries 1−5). High yield of the product was obtained in the presence of K_2CO_3 as the base when compared to other bases (Cs_2CO_3, NaOH, and Et_3N) (Table S2, entries 6−8).

Influence of the light source on the Sonogashira reaction was also established in the presence of the synthesized catalyst. The product yield was very low in dark at RT and moderate (59%) at 60 °C. Under vis light (Hg lamp 250W), the yield was 81%,

Table 2. Substrate Scope of the SCR Catalyzed by $NiFe_2O_4$@TiO_2@PDA-Pd under Sunlight Irradiation[a]

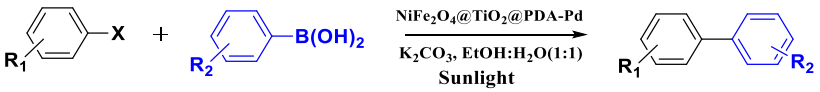

S. No.	Aryl halides	Arylboronic acid	Time (h)	Yield (%)[b]
1	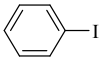	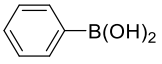	**0.5**	**98**
2	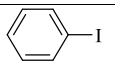	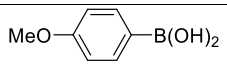	**0.5**	**92**
3	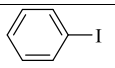	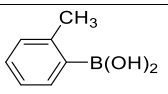	**1**	**82**
4	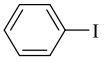	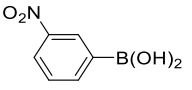	**1**	**75**
5	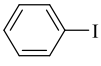	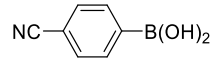	**1**	**85**
6	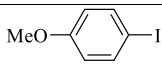	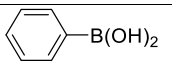	**0.5**	**96**
7	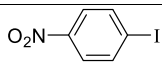	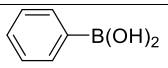	**0.5**	**92**
8	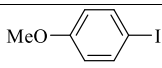	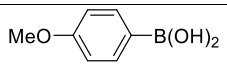	**0.5**	**95**
9	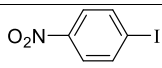	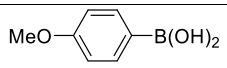	**0.5**	**93**
10	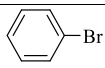	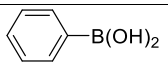	**2**	**80**
11	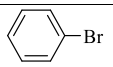	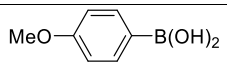	**2**	**76**
12	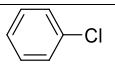	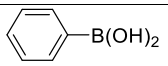	**4**	**52**

[a]Reaction conditions: aryl halide (1.0 mmol), phenyl boronic acid (1.5 mmol), $NiFe_2O_4$@TiO_2@PDA-Pd catalyst (5 mg), and K_2CO_3 (2.5 mmol) in EtOH·H_2O (3 mL) under sunlight at 30 °C. [b]Isolated yields.

https://doi.org/10.1021/acsomega.2c03603
ACS Omega 2022, 7, 29356−29368

Table 3. Substrate Scope of the Sonogashira Coupling Reaction Catalyzed by $NiFe_2O_4$@TiO_2@PDA-Pd under Sunlight Irradiation[a]

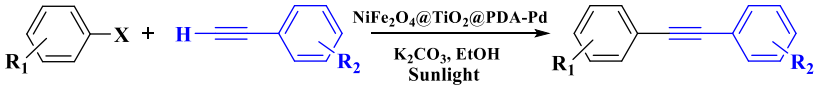

S. No.	Aryl halides	Arylacetylenes	Time (hrs)	Yield (%)[b]
1	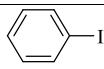	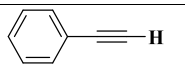	2.5	96
2	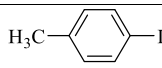	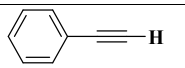	3	94
3	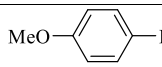	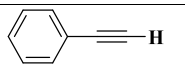	3	93
4	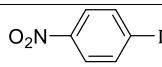	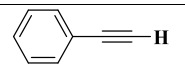	3	90
5		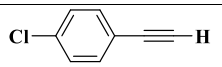	3	92
6	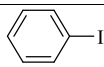	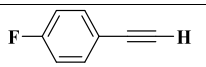	3	88
7	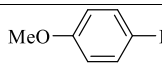	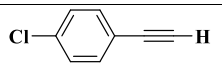	3	90
8	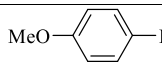	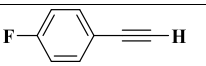	3	85
9		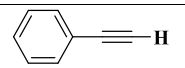	4	85
10	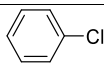	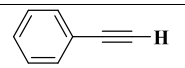	5.5	60

[a]Reaction conditions: aryl halide (1.0 mmol), phenyl acetylene (1.3 mmol), $NiFe_2O_4$@TiO_2@PDA-Pd catalyst (10 mg), and K_2CO_3 (2 mmol) in EtOH (3 mL) under sunlight at 30 °C. [b]Isolated yields.

and under sunlight, higher yield (96%) was obtained (Table S2, entries 9−11). Thus, the fact of using sunlight in getting high yield was established. The feasibility of the Sonogashira reaction was verified with $NiFe_2O_4$, $NiFe_2O_4$@TiO_2, and $NiFe_2O_4$@TiO_2@PDA separately, and no products were observed.

The substrate scope of the Sonogashira coupling reaction over the $NiFe_2O_4$@TiO_2@PDA-Pd nanophotocatalyst was also investigated using the optimized conditions. The aryl halides with EWGs or EDGs have resulted in a higher yield of the product (Table 3).

The efficacy of the catalyst was compared with that of already reported catalysts for Suzuki and Sonogashira coupling reactions (Table S3). It is evident from Table S3 that our proposed $NiFe_2O_4$@TiO_2@PDA-Pd nanophotocatalyst acts efficiently in producing the desired products in both Suzuki and Sonogashira coupling reactions with an excellently good yield (98 and 96%) in short reaction time (0.5 and 2.5 h) under natural sunlight. Thus, our catalyst shows its supremacy in its activity among other reported systems.

3.4. Stability and Recyclability of the Catalyst. Two significant parameters to be examined while evaluating a photocatalytic reaction are photo-stability and recyclability. The photo-stability and recyclability of our $NiFe_2O_4$@TiO_2@PDA-Pd catalyst in photocatalytic Suzuki and Sonogashira coupling reactions were investigated in this study. Owing to the magnetic nature of the photocatalyst, it was retrieved from the reaction mixture in a simple manner with the aid of an external magnet after each cycle. The magnetically retrieved catalyst was washed with EtOH and dried, and its catalytic performance was assessed in the next run. Figure 5 shows the reuse of the recovered catalyst five times without any substantial loss of its photocatalytic activity, indicating the good stability of the catalyst.

Many heterogeneous catalysts have leaching issues, and the leached Pd NPs into the solution lead to the decrease in the Pd content in the catalyst which was mainly responsible for its activity. To test the Pd leaching, ICP-OES analysis of the recovered catalyst was performed. It was observed that the Pd content of the nanocatalyst had decreased from (3.61) wt % to (2.26) wt % in the Suzuki reaction and to (2.45) wt % in the Sonogashira reaction after five time use. To further confirm the recyclable nature of the magnetic reusable catalyst, XRD analysis and FT-IR analysis on the recovered photocatalyst were performed. Figure S1 shows the XRD spectra of the $NiFe_2O_4$@TiO_2@PDA-Pd photocatalyst after five times of reused experiments. No impurity peaks were detected in the XRD spectra of the reused photocatalyst, thus confirming the stability and recyclability of the catalyst. Furthermore, FT-IR analysis of the photocatalyst after five cycles of reuse was

https://doi.org/10.1021/acsomega.2c03603
ACS Omega 2022, 7, 29356−29368

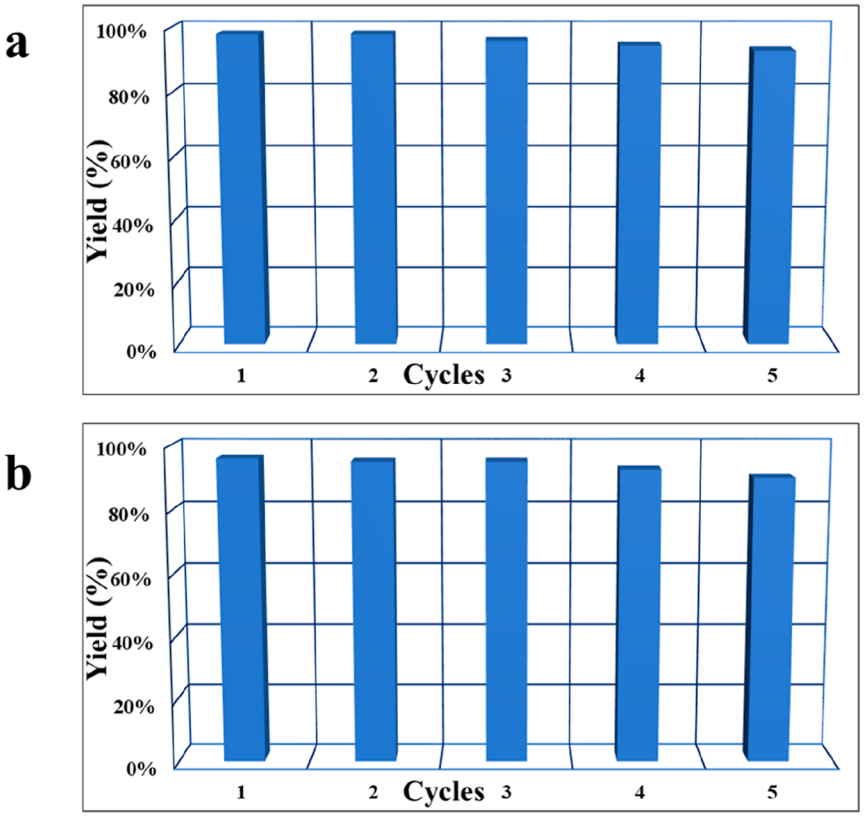

Figure 5. Recyclability of $NiFe_2O_4$@TiO_2@PDA-Pd for photocatalytic activity. (a) Suzuki and (b) Sonogashira reactions.

performed where it confirmed the fact that absorption peaks of the reused catalyst are intact like those of the fresh catalyst (Figure S2).

3.5. Heterogeneity of the Catalyst. Heterogeneity of the designed catalyst was tested via the hot filtration method and leaching test. In this method, Suzuki and Sonogashira coupling reactions were carried out separately in the presence of the synthesized photocatalyst $NiFe_2O_4$@TiO_2@PDA-Pd in direct sunlight under optimum reaction conditions. The SCR was carried out for 15 min (half the reaction time) under the reaction conditions, and subsequently, the reaction mixture was separated into two equal halves. From one half of the reaction mixture, the catalyst was separated and retrieved employing an external magnet, and the reaction was allowed to continue in both portions for an extra 15 min. In the same way, the Sonogashira coupling reaction was also performed using the prepared catalyst under optimal conditions for 90 min in sunlight, followed by the separation of the reaction mixture into two equal halves. By following the aforementioned procedure, the catalyst in one part is magnetically separated, and the reaction in both halves was allowed to progress for extra 60 min. From both the coupling reactions, it is evident that in the absence of the catalyst, no further progress in the reaction was observed, whereas the other half portion of the reaction mixture, in the absence of the catalyst, has progressed to the complete conversion of the substrates into desired products, as mentioned in the Figure S3. This infers the fact that there is trivial leaching of Pd into the reaction mixture, confirming the heterogeneity of the developed catalyst. Furthermore, Pd leaching from the catalyst was also assessed by ICP-OES analysis which confirmed the Pd leaching to be <0.2% (nominal).

3.6. Active Species Trapping Experiment. Active species trapping experiments were performed using scavengers to understand the role of photogenerated active species (e^-–h^+ pair) in the photocatalytic mechanism of the $NiFe_2O_4$@TiO_2@PDA-Pd photocatalyst. In this experiment, $K_2S_2O_8$ was used as an e^- scavenger, and ammonium oxalate (AO) was used as a h^+ scavenger. In the presence of $K_2S_2O_8$, poor yield (38%) of the product was observed (Table S1, entry 18), whereas in the presence of AO, 51% yield of the product was observed (Table S1, entry 19). Thus, the trapping experiments indicate that both the photogenerated active species play a significant role in the C−C coupling reaction with a major contribution from photogenerated electrons.

3.7. Photocatalytic Mechanism of Suzuki and Sonogashira Coupling Reactions. A plausible photocatalytic mechanism for the Suzuki and Sonogashira coupling reactions in the presence of the $NiFe_2O_4$@TiO_2@PDA-Pd photocatalyst was proposed based on the performed experimental observations and previously reported data.[47−49] Simulated visible light irradiation of the catalyst led to the simultaneous formation of photogenerated electrons (e^-) and holes (h^+) in $NiFe_2O_4$ and TiO_2, as illustrated in Figure 6. It is because light irradiation led to the promotion of an e^- from the valence band (VB) to the conduction band (CB) leaving a h^+ in the VB. Thus, photogenerated e^-–h^+ pairs are formed simultaneously in $NiFe_2O_4$ and TiO_2. The photogenerated e^- from the CB of $NiFe_2O_4$ can be easily transferred to the CB of TiO_2 by the simultaneous transfer of photogenerated h^+ from the VB of TiO_2 to the VB of $NiFe_2O_4$. This is ascribed to the more negative CB potential of $NiFe_2O_4$ than that of TiO_2 and more positive VB potential of TiO_2 than that of $NiFe_2O_4$. Furthermore, it is also evident by the fact that the combination

https://doi.org/10.1021/acsomega.2c03603
ACS Omega 2022, 7, 29356−29368

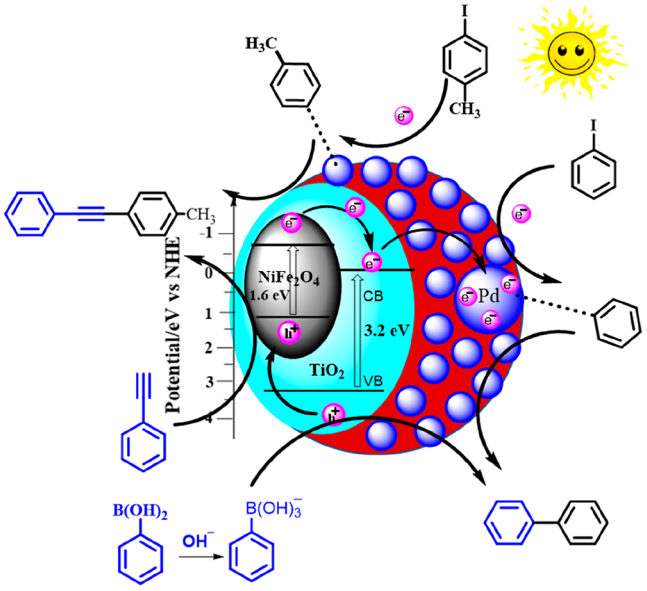

Figure 6. Plausible photocatalytic mechanism over the $NiFe_2O_4$@TiO_2@PDA-Pd nanophotocatalyst of Suzuki and Sonogashira coupling reactions.

of $NiFe_2O_4$ and TiO_2 develops interfacial contact between them, thus creating a pathway for easy transfer of e^- from the CB of $NiFe_2O_4$ to the CB of TiO_2 and therefore hinders the e^-–h^+ pair recombination. The photogenerated e^- available in the CB of TiO_2 will be transported through the PDA layer to the Pd surface. Active Pd NPs act as electron reservoirs and thus trap the electrons reaching their surface. These photogenerated electrons and Pd NPs act as active sites and attack the C–X bond of the adsorbed aryl halides forming the aryl–Pd complex via oxidative addition. On the other hand, arylboronic acid combines with OH^- in a basic reaction medium to produce aryl-$B(OH)_3^-$. Furthermore, C–B bond cleavage occurs to generate the biaryl–Pd complex in the presence of h^+ (transmetalation). In the final step, a biaryl product is obtained via reductive elimination.[50,51]

For the Sonogashira coupling reaction also, the photogenerated electrons and Pd NPs act as active sites attacking the C–X bond of the adsorbed aryl halide and resulting in the aryl–Pd complex. Simultaneously, photogenerated holes attract the electronic clouds of the alkyne units in phenyl acetylene, making the terminal ^{sp}C–H more acidic. Then, K_2CO_3 deprotonates terminal H of the alkyne unit, and the resulting species combines with the aryl–Pd complex to form an alkynated Pd complex. In the final reductive elimination step, diarylacetylene is formed.[52,53]

The proposed mechanism reveals the uniqueness of the synthesized photocatalyst as a sole catalyst for both Suzuki and Sonogashira coupling reactions under sunlight irradiation.

4. CONCLUSIONS

In summary, we have designed and developed a magnetically recyclable Pd-supported PDA-coated core@shell $NiFe_2O_4$@TiO_2 nanocatalyst, with good photocatalytic activity for both Suzuki and Sonogashira coupling reactions under sunlight irradiation under ambient conditions. The activity of the catalyst was validated for both coupling reactions, and its effectiveness for reactions involving a variety of substrates under sunlight irradiation to yield biaryls and diarylacetylenes was tested. The reactions were facilitated by low Pd loading in the presence of eco-friendly polar protic solvents (ethanolic water/ethanol) in a very short reaction duration with an excellent yield (96–98%). The catalyst is validated for substituted substrates in both Suzuki and Sonogashira reactions to give a good yield of the product, indicating its efficacy. The plausible mechanism has been proposed for the coupling reactions where the simultaneous utilization of both the photogenerated e^-–h^+ pairs in various steps of the coupling reactions denotes an exceptional catalytic view point of the catalyst. The catalyst was retrieved with the aid of an external magnet and was reutilized for five cycles. ICP-OES analysis indicated the stability of the catalyst without considerable loss after reusing five times which was further confirmed by FTIR and XRD analysis. It was found that the $NiFe_2O_4$@TiO_2@PDA-Pd nanophotocatalyst exhibits greater activity with high yield in comparison to a number of reported catalysts.

■ ASSOCIATED CONTENT

Supporting Information

The Supporting Information is available free of charge at https://pubs.acs.org/doi/10.1021/acsomega.2c03603.

Screening of reaction conditions for Suzuki and Sonogashira coupling reactions; XRD and FTIR spectra of reused catalysts; hot filtration and the leaching test of the $NiFe_2O_4$@TiO_2@PDA-Pd catalyst for Suzuki and Sonogashira coupling reactions; comparison of the $NiFe_2O_4$@TiO_2@PDA-Pd catalyst with other previously reported catalysts; and characterization data of products along with copies of ^1H and ^{13}C NMR spectra (PDF)

■ AUTHOR INFORMATION

Corresponding Author

Raghasudha Mucherla − *Department of Chemistry, National Institute of Technology Warangal, Warangal 506 004 Telangana, India;* orcid.org/0000-0002-1710-9630; Phone: (+91) 9550083100; Email: raghas13@nitw.ac.in

Author

Prashanth Goud Banda − *Department of Chemistry, National Institute of Technology Warangal, Warangal 506 004 Telangana, India*

Complete contact information is available at: https://pubs.acs.org/10.1021/acsomega.2c03603

Author Contributions

M.R. and B.P.G. designed and developed the photocatalyst and validated its activity for coupling reactions. The manuscript was written through contributions of all the authors. All the authors have given approval for the final version.

Notes

The authors declare no competing financial interest.

■ ACKNOWLEDGMENTS

Author M.R. is grateful to the National Institute of Technology Warangal (NITW) for the Research Seed Money (P1082 Plan Gen.-RSM), the DST-FIST grant, and SR/FST/CSII/2018/65 awarded to Department of Chemistry, NITW, for the financial support of this work. B.P.G. is grateful to NITW for the Senior Research Fellowship.

REFERENCES

(1) Ong, W. J. Learning from Natural Leaves: Going Green with Artificial Photosynthesis Forum. *ACS Appl. Mater. Interfaces* **2019**, *11*, 5579−5580.

(2) Linic, S.; Christopher, P.; Ingram, D. B. Plasmonic-Metal Nanostructures for Efficient Conversion of Solar to Chemical Energy. *Nat. Mater.* **2011**, *10*, 911−921.

(3) Wang, F.; Li, C.; Chen, H.; Jiang, R.; Sun, L. D.; Li, Q.; Wang, J.; Yu, J. C.; Yan, C. H. Plasmonic Harvesting of Light Energy for Suzuki Coupling Reactions. *J. Am. Chem. Soc.* **2013**, *135*, 5588−5601.

(4) Yu, C.; Li, G.; Kumar, S.; Yang, K.; Jin, R. Phase Transformation Synthesis of Novel Ag2O/Ag2CO3Heterostructures with High Visible Light Efficiency in Photocatalytic Degradation of Pollutants. *Adv. Mater.* **2014**, *26*, 892−898.

(5) Li, X. H.; Antonietti, M. Metal nanoparticles at mesoporous N-doped carbons and carbon nitrides: functional Mott-Schottky heterojunctions for catalysis. *Chem. Soc. Rev.* **2013**, *42*, 6593−6604.

(6) Long, R.; Rao, Z.; Mao, K.; Li, Y.; Zhang, C.; Liu, Q.; Wang, C.; Li, Z. Y.; Wu, X.; Xiong, Y. Efficient Coupling of Solar Energy to Catalytic Hydrogenation by Using Well-Designed Palladium Nanostructures. *Angew. Chem., Int. Ed.* **2015**, *54*, 2425−2430.

(7) Yang, X.; Zhang, S.; Li, P.; Gao, S.; Cao, R. Visible-Light-Driven Photocatalytic Selective Organic Oxidation Reactions. *J. Mater. Chem. A* **2020**, *8*, 20897−20924.

(8) Kim, J. H.; Lee, M.; Lee, J. S.; Park, C. B. Self-Assembled Light-Harvesting Peptide Nanotubes for Mimicking Natural Photosynthesis. *Angew. Chem., Int. Ed.* **2012**, *51*, 517−520.

(9) Li, X. H.; Chen, J. S.; Wang, X.; Sun, J.; Antonietti, M. Metal-Free Activation of Dioxygen by Graphene/g-C3N4 Nanocomposites: Functional Dyads for Selective Oxidation of Saturated Hydrocarbons. *J. Am. Chem. Soc.* **2011**, *133*, 8074−8077.

(10) Nguyen, C. C.; Vu, N. N.; Do, T. O. Recent Advances in the Development of Sunlight-Driven Hollow Structure Photocatalysts and Their Applications. *J. Mater. Chem. A* **2015**, *3*, 18345−18359.

(11) Kou, J.; Lu, C.; Wang, J.; Chen, Y.; Xu, Z.; Varma, R. S. Selectivity Enhancement in Heterogeneous Photocatalytic Transformations. *Chem. Rev.* **2017**, *117*, 1445−1514.

(12) Elhage, A.; Lanterna, A. E.; Scaiano, J. C. Light-Induced Sonogashira C-C Coupling under Mild Conditions Using Supported Palladium Nanoparticles. *ACS Sustainable Chem. Eng.* **2018**, *6*, 1717−1722.

(13) Shafiei, N.; Nasrollahzadeh, M.; Baran, T.; Baran, N. Y.; Shokouhimehr, M. Pd Nanoparticles Loaded on Modified Chitosan-Unye Bentonite Microcapsules: A Reusable Nanocatalyst for Sonogashira Coupling Reaction. *Carbohydr. Polym.* **2021**, *262*, 117920.

(14) Baran, T.; Akay, S.; Kayan, B. Fabrication of Palladium Nanoparticles Supported on Natural Volcanic Tuff/Fe3O4 and Its Catalytic Role in Microwave-Assisted Suzuki-Miyaura Coupling Reactions. *Catal. Lett.* **2021**, *151*, 1102−1110.

(15) Nasrollahzadeh, M.; Motahharifar, N.; Ghorbannezhad, F.; Soheili Bidgoli, N. S.; Baran, T.; Varma, R. S. Recent Advances in Polymer Supported Palladium Complexes as (Nano)Catalysts for Sonogashira Coupling Reaction. *Mol. Catal.* **2020**, *480*, 110645.

(16) D'Alterio, M. C.; Casals-Cruañas, È.; Tzouras, N. V.; Talarico, G.; Nolan, S. P.; Poater, A. Mechanistic Aspects of the Palladium-Catalyzed Suzuki-Miyaura Cross-Coupling Reaction. *Chem.—Eur. J.* **2021**, *27*, 13481−13493.

(17) Fusini, G.; Rizzo, F.; Angelici, G.; Pitzalis, E.; Evangelisti, C.; Carpita, A. Polyvinylpyridine-Supported Palladium Nanoparticles: An Efficient Catalyst for Suzuki-Miyaura Coupling Reactions. *Catalysts* **2020**, *10*, 330.

(18) Çalışkan, M.; Baran, T. Facile Synthesis of Biaryls by Palladium Nanoparticles Adorned on Kaolin/$NiFe_2O_4$ Composite as a Magnetically Retrievable Nanocatalyst. *Colloids Interface Sci. Commun.* **2021**, *43*, 100445.

(19) Orooji, Y.; Pakzad, K.; Nasrollahzadeh, M.; Tajbakhsh, M. Novel Magnetic Lignosulfonate-Supported Pd Complex as an Efficient Nanocatalyst for N-Arylation of 4-Methylbenzenesulfonamide. *Int. J. Biol. Macromol.* **2021**, *182*, 564−573.

(20) Nasrollahzadeh, M.; Bidgoli, N. S. S.; Issaabadi, Z.; Ghavamifar, Z.; Baran, T.; Luque, R. L. Hibiscus Rosasinensis L. aqueous extract-assisted valorization of lignin: Preparation of magnetically reusable Pd NPs@Fe3O4-lignin for Cr(VI) reduction and Suzuki-Miyaura reaction in eco-friendly media. *Int. J. Biol. Macromol.* **2020**, *148*, 265−275.

(21) Baran, T.; Nasrollahzadeh, M. Cyanation of Aryl Halides and Suzuki-Miyaura Coupling Reaction Using Palladium Nanoparticles Anchored on Developed Biodegradable Microbeads. *Int. J. Biol. Macromol.* **2020**, *148*, 565−573.

(22) Zhang, S.; Chang, C.; Huang, Z.; Ma, Y.; Gao, W.; Li, J.; Qu, Y. Visible-Light-Activated Suzuki-Miyaura Coupling Reactions of Aryl Chlorides over the Multifunctional Pd/Au/Porous Nanorods of CeO2 Catalysts. *ACS Catal.* **2015**, *5*, 6481−6488.

(23) Parasram, M.; Gevorgyan, V. Visible Light-Induced Transition Metal-Catalyzed Transformations: Beyond Conventional Photosensitizers. *Chem. Soc. Rev.* **2017**, *46*, 6227−6240.

(24) Schneider, J.; Matsuoka, M.; Takeuchi, M.; Zhang, J.; Horiuchi, Y.; Anpo, M.; Bahnemann, D. W. Understanding TiO2 Photocatalysis: Mechanisms and Materials. *Chem. Rev.* **2014**, *114*, 9919−9986.

(25) Ghosh, B. K.; Moitra, D.; Chandel, M.; Ghosh, N. N. Preparation of TiO2/Cobalt Ferrite/Reduced Graphene Oxide Nanocomposite Based Magnetically Separable Catalyst with Improved Photocatalytic Activity. *J. Nanosci. Nanotechnol.* **2017**, *17*, 4694−4703.

(26) Ghosh, B. K.; Moitra, D.; Chandel, M.; Lulla, H.; Ghosh, N. N. Ag nanoparticle immobilized mesoporous TiO2-cobalt ferrite nanocatalyst: A highly active, versatile, magnetically separable and reusable catalyst. *Mater. Res. Bull.* **2017**, *94*, 361−370.

(27) Liu, H.; Jia, Z.; Ji, S.; Zheng, Y.; Li, M.; Yang, H. Synthesis of TiO2/SiO2@Fe3O4 magnetic microspheres and their properties of photocatalytic degradation dyestuff. *Catal. Today* **2011**, *175*, 293−298.

(28) Gao, X.; Liu, X.; Zhu, Z.; Wang, X.; Xie, Z. Enhanced Photoelectrochemical and Photocatalytic Behaviors of MFe_2O_4 (M = Ni, Co, Zn and Sr) Modified TiO_2 Nanorod Arrays. *Sci. Rep.* **2016**, *6*, 30543.

(29) Huang, S.; Xu, Y.; Zhou, T.; Xie, M.; Ma, Y.; Liu, Q.; Jing, L.; Xu, H.; Li, H. Constructing magnetic catalysts with in-situ solid-liquid interfacial photo-Fenton-like reaction over Ag3PO4@NiFe2O4 composites. *Appl. Catal., B* **2018**, *225*, 40−50.

(30) Zhu, H. Y.; Jiang, R.; Fu, Y. Q.; Li, R. R.; Yao, J.; Jiang, S. T. Novel multifunctional NiFe 2 O 4 /ZnO hybrids for dye removal by adsorption, photocatalysis and magnetic separation. *Appl. Surf. Sci.* **2016**, *369*, 1−10.

(31) Wang, B.; Guo, X.; Jin, G.; Guo, X. Visible-Light-Enhanced Photocatalytic Sonogashira Reaction over Silicon Carbide Supported Pd Nanoparticles. *Catal. Commun.* **2017**, *98*, 81−84.

(32) Elhage, A.; Lanterna, A. E.; Scaiano, J. C. Tunable Photocatalytic Activity of Palladium-Decorated TiO2: Non-Hydrogen-Mediated Hydrogenation or Isomerization of Benzyl-Substituted Alkenes. *ACS Catal.* **2017**, *7*, 250−255.

(33) Feizi Mohazzab, B.; Jaleh, B.; Issaabadi, Z.; Nasrollahzadeh, M.; Varma, R. S. Stainless Steel Mesh-GO/Pd NPs: Catalytic Applications of Suzuki-Miyaura and Stille Coupling Reactions in Eco-Friendly Media. *Green Chem.* **2019**, *21*, 3319−3327.

(34) Khazaei, A.; Khazaei, M.; Nasrollahzadeh, M. Nano-Fe 3 O 4 @ SiO 2 supported Pd(0) as a magnetically recoverable nanocatalyst for Suzuki coupling reaction in the presence of waste eggshell as low-cost natural base. *Tetrahedron* **2017**, *73*, 5624−5633.

(35) Liu, R.; Guo, Y.; Odusote, G.; Qu, F.; Priestley, R. D. Core-Shell Fe3O4 Polydopamine Nanoparticles Serve Multipurpose as Drug Carrier, Catalyst Support and Carbon Adsorbent. *ACS Appl. Mater. Interfaces* **2013**, *5*, 9167−9171.

(36) Li, H.; Xi, J.; Donaghue, A. G.; Keum, J.; Zhao, Y.; An, K.; McKenzie, E. R.; Ren, F. Synthesis and Catalytic Performance of

https://doi.org/10.1021/acsomega.2c03603
ACS Omega 2022, 7, 29356−29368

Polydopamine Supported Metal Nanoparticles. *Sci. Rep.* **2020**, *10*, 10416.
(37) Ju, P.; Wu, S.; Su, Q.; Li, X.; Liu, Z.; Li, G.; Wu, Q. Salen-Porphyrin-Based Conjugated Microporous Polymer Supported Pd Nanoparticles: Highly Efficient Heterogeneous Catalysts for Aqueous C-C Coupling Reactions. *J. Mater. Chem. A* **2019**, *7*, 2660−2666.
(38) Laokul, P.; Amornkitbamrung, V.; Seraphin, S.; Maensiri, S. Characterization and Magnetic Properties of Nanocrystalline $CuFe_2O_4$, $NiFe_2O_4$, $ZnFe_2O_4$ Powders Prepared by the Aloe Vera Extract Solution. *Curr. Appl. Phys.* **2011**, *11*, 101−108.
(39) Liu, Y.; Cherkasov, N.; Gao, P.; Fernández, J.; Lees, M. R.; Rebrov, E. V. The enhancement of direct amide synthesis reaction rate over TiO 2 @SiO 2 @NiFe 2 O 4 magnetic catalysts in the continuous flow under radiofrequency heating. *J. Catal.* **2017**, *355*, 120−130.
(40) Farzad, E.; Veisi, H. Fe 3 O 4 /SiO 2 nanoparticles coated with polydopamine as a novel magnetite reductant and stabilizer sorbent for palladium ions: Synthetic application of Fe 3 O 4 /SiO 2 @PDA/Pd for reduction of 4-nitrophenol and Suzuki reactions. *J. Ind. Eng. Chem.* **2018**, *60*, 114−124.
(41) Veisi, H.; Sarachegol, P.; Hemmati, S. Palladium(II) anchored on polydopamine coated-magnetic nanoparticles (Fe3O4@PDA@Pd(II)): A heterogeneous and core-shell nanocatalyst in Buchwald-Hartwig C-N cross coupling reactions. *Polyhedron* **2018**, *156*, 64−71.
(42) Rohani, S.; Ziarati, A.; Ziarani, G. M.; Badiei, A.; Burgi, T. Engineering of highly active Au/Pd supported on hydrogenated urchin-like yolk@shell TiO2 for visible light photocatalytic Suzuki coupling. *Catal. Sci. Technol.* **2019**, *9*, 3820−3827.
(43) Manna, J.; Akbayrak, S.; Özkar, S. Palladium(0) nanoparticles supported on polydopamine coated Fe3O4 as magnetically isolable, highly active and reusable catalysts for hydrolytic dehydrogenation of ammonia borane. *RSC Adv.* **2016**, *6*, 102035−102042.
(44) Babu, B.; Koutavarapu, R.; Shim, J.; Kim, J.; Yoo, K. Improved Sunlight-Driven Photocatalytic Abatement of Tetracycline and Photoelectrocatalytic Water Oxidation by Tin Oxide Quantum Dots Anchored on Nickel Ferrite Nanoplates. *J. Electroanal. Chem.* **2021**, *900*, 115699.
(45) Van Tran, C.; La, D. D.; Thi Hoai, P. N.; Ninh, H. D.; Thi Hong, P. N.; Vu, T. H. T.; Nadda, A. K.; Nguyen, X. C.; Nguyen, D. D.; Ngo, H. H. New TiO2-doped Cu-Mg spinel-ferrite-based photocatalyst for degrading highly toxic rhodamine B dye in wastewater. *J. Hazard. Mater.* **2021**, *420*, 126636.
(46) Duarah, R.; Karak, N. Hyperbranched Polyurethane/Palladium-Reduced Carbon Dot Nanocomposite: An Efficient and Reusable Mesoporous Catalyst for Visible-Light-Driven C-C Coupling Reactions. *Ind. Eng. Chem. Res.* **2019**, *58*, 16307−16319.
(47) Li, Y.; Zhang, Z.; Pei, L.; Li, X.; Fan, T.; Ji, J.; Shen, J.; Ye, M. Multifunctional photocatalytic performances of recyclable Pd-NiFe 2 O 4 /reduced graphene oxide nanocomposites via different co-catalyst strategy. *Appl. Catal., B* **2016**, *190*, 1−11.
(48) He, Z.; Xia, Y.; Tang, B.; Su, J. Fabrication and photocatalytic property of magnetic NiFe2O4/Cu2O composites. *Mater. Res. Express* **2017**, *4*, 095501.
(49) Jiang, J.; Chen, Z.; Wang, P.; Gu, P. Y.; Liu, J.; Zhang, Z.; Xu, Q. Preparation of black hollow TiO2 nanotube-coated PDA@Ag2S heterostructures for efficient photocatalytic reduction of Cr(VI). *J. Solid State Chem.* **2022**, *307*, 122865.
(50) Fu, W.; Xu, X.; Wang, W.; Shen, J.; Ye, M. In-Situ Growth of NiFe2O4/2D MoS2 p-n Heterojunction Immobilizing Palladium Nanoparticles for Enhanced Visible-Light Photocatalytic Activities. *ACS Sustainable Chem. Eng.* **2018**, *6*, 8935−8944.
(51) Xiao, Q.; Sarina, S.; Jaatinen, E.; Jia, J.; Arnold, D. P.; Liu, H.; Zhu, H. Efficient Photocatalytic Suzuki Cross-Coupling Reactions on Au-Pd Alloy Nanoparticles under Visible Light Irradiation. *Green Chem.* **2014**, *16*, 4272−4285.
(52) Nath, I.; Chakraborty, J.; Khan, A.; Arshad, M. N.; Azum, N.; Rab, M. A.; Asiri, A. M.; Alamry, K. A.; Verpoort, F. Conjugated mesoporous polyazobenzene-Pd(II) composite: A potential catalyst for visible-light-induced Sonogashira coupling. *J. Catal.* **2019**, *377*, 183−189.
(53) Wang, B.; Wang, Y.; Li, J.; Guo, X.; Bai, G.; Tong, X.; Jin, G.; Guo, X. Photocatalytic Sonogashira Reaction over Silicon Carbide Supported Pd-Cu Alloy Nanoparticles under Visible Light Irradiation. *Catal. Sci. Technol.* **2018**, *8*, 3357−3362.

https://doi.org/10.1021/acsomega.2c03603
ACS Omega 2022, 7, 29356−29368